J. Electrochem. Sci. Eng. **15(4)** (2025) 2715; http://dx.doi.org/10.5599/jese.2715

Open Access : : ISSN 1847-9286
https://pub.iapchem.org/ojs/index.php/JESE

Original scientific paper

CuO-based nanocomposite: synthesis, characterization, and evaluation of the corrosion inhibition effectiveness for mild steel in HCl

Msenhemba Moses Mchihi[1,2], Abimbola Modupe Olatunde[1] and Nnenna Winifred Odozi[1,✉]

[1]*Department of Chemistry, Faculty of Science, University of Ibadan, Ibadan, Nigeria*
[2]*Department of Chemical Science, School of Science, Yaba College of Technology Lagos, Nigeria*

Corresponding author: ✉ nw.odozi@gmail.com

Received: March 17, 2025; Accepted: May 27, 2025; Published: June 6, 2025

Abstract

Mitigating mild steel (MS) deterioration within acidic environments is critical for minimizing economic losses. CuO nanoparticles/arginine/tyrosine (CAT) was synthesized by modifying CuO nanoparticles with a 10.0 % solution of each arginine and tyrosine, through the use of ultrasonication. The characterization of CAT was conducted utilizing X-ray diffraction (XRD), Fourier-transform infrared spectroscopy, transmission electron microscopy and Brunauer-Emmett-Teller analysis. To investigate MS corrosion in 1.0 M HCl, both potentiodynamic polarization and electrochemical impedance spectroscopy techniques were employed. The XRD results indicated the presence of distinct peaks, confirming the crystalline structure of CAT, with an average crystallite size equal to 39.5 nm. The FTIR band observed within the range of 580-610 cm^{-1} is likely attributable to Cu-O stretching vibrations. TEM imaging demonstrated that CAT comprises spherical and well-dispersed particles. Furthermore, the surface area of CAT was determined to be 221 m^2 g^{-1}, with a pore diameter of 2.137 nm, indicating its mesoporous nature. The variation in corrosion potential was below 85 mV, indicating that CAT functioned as a mixed-type inhibitor. The charge transfer resistance rose from 7.3 Ω cm^2 without CAT to 226.8 Ω cm^2 at 1000 ppm of CAT, demonstrating the potential of CAT as an inhibitor for MS corrosion in HCl. CuO, arginine, and tyrosine exhibit HOMO and LUMO properties that could play a significant role in corrosion inhibition.

Keywords

Copper oxide nanoparticles; low carbon steel; corrosion protection; arginine-tyrosine functionalization

Introduction

Due to its accessibility, relatively low cost, and effectiveness, hydrochloric acid is frequently utilized in various industrial applications, including acid pickling, cleaning, and descaling of mild

steel. However, the corrosive properties of concentrated hydrochloric acid can lead to significant deterioration of mild steel [1,2]. The corrosion of metals represents a critically significant issue that has led to substantial economic losses across diverse industrial and construction sectors [3]. The use of corrosion inhibitors has proven effective for corrosion mitigation in diverse media. The application of corrosion inhibitors represents a potentially simple, rapid, cost-effective, environmentally sustainable, and highly efficient approach to mitigate corrosion of metals and alloys in numerous media [4,5]. They enhance the longevity of equipment in aggressive environments, allow low-cost steel to be employed instead of expensive corrosion-resistant alloys, and reduce economic and health hazards. Environmental regulatory bodies in various nations have enacted strict regulations and rules pertaining to the use and expulsion of corrosion inhibitors, considering toxicity, bioaccumulation, and biodegradability conditions, which provokes the search for novel corrosion inhibitors with negligible or no toxicity. Some corrosion inhibitors are currently banned in other countries due to their high toxicity. For instance, pigments containing chromium, such as strontium chromate [6] and zinc chromate, have been comprehensively used for a long time as anticorrosive pigments with excellent corrosion inhibitive performance. Sadly, chromium (VI) is carcinogenic due to its high tendency to oxidize organic molecules, provoking its restriction [7,8]. In addition to chromate, the high toxicity associated with phosphate and arsenic compounds has prompted the establishment of stringent international regulations that limit their usage. This has consequently heightened the demand for alternative inhibitors with comparable anticorrosive qualities while addressing environmental and health issues [5]. The corrosion inhibitor market is projected to expand from an estimated USD 7.9 billion in 2021 to USD 10.1 billion by 2026, reflecting a compound annual growth rate of 4.9 % [5].

The corrosion inhibitory effect of plant extracts [9-13], nanomaterials [14-16], organic compounds [17,18], and inorganic compounds [19,20] has been reported. The majority of inorganic compounds employed as corrosion inhibitors are toxic and difficult to synthesize. The drawbacks of using plant extracts as corrosion inhibitors include limited solubility in polar electrolytes (predominantly at higher concentrations), wearisome biodegradability, difficult extraction protocols, and the use of toxic solvents that affect the environment after their expulsion [16,21]. Due to the intricate nature of synthesis procedures and elevated expenses, the application of organically synthesized compounds, such as ionic liquids or drugs, for corrosion inhibition may prove to be economically unfeasible [18].

Metal oxide nanoparticles (such as nanoparticles of ZnO, CuO, Fe_2O_3 and NiO) are receiving tremendous attention in corrosion inhibition due to their high surface-to-volume ratio and high surface area compared to their bulk counterparts, along with their interesting mechanical, electronic, structural, optical and thermal properties [22,23]. A nanomaterial is a material that has its size or at least one dimension in the nanoscale range of 1 to 100 nm [23]. Nanoparticles are known to block active sites on a metal surface, resulting in a considerable decrease in corrosion rates [24]. However, metal oxide nanoparticles have some limitations arising from their tendency to agglomerate. There are reports on synthesis of metal oxide nanoparticles for various applications. However, there is a paucity of information on minimizing agglomeration of metal oxide nanoparticles through functionalization for enhanced efficacy.

Aslam *et al.* [14] reported the synthesis of ZrO_2 nanoparticles functionalized with glycine as a corrosion inhibitor for mild steel in acidic medium. The zirconium oxide nanoparticle/glycine nanocomposite demonstrated good performance as a corrosion inhibitor for mild steel in acidic medium. Compounds consisting of numerous heteroatoms such as nitrogen, oxygen and sulfur are

known to be efficient corrosion inhibitors, especially in acidic media. To this end, metal oxide nanoparticles functionalized with arginine and tyrosine could offer better protection against mild steel corrosion. Findings from a comparative computational analysis of the inhibitory efficiency of the 20 L-amino acids corroborate this notion [25]. Therefore, this study was designed to prepare CuO nanoparticles/arginine/tyrosine (CAT) nanocomposite, followed by its characterization and application as a corrosion inhibitor for mild steel in 1 M hydrochloric acid.

Experimental

Synthesis of CuO nanoparticles/arginine/tyrosine nanocomposite

Reagents employed in this study were purchased from commercial suppliers and used without further purification. The procedure reported by Aslam *et al.* [14] was reformed and utilised for the synthesis of CuO nanoparticles/arginine/tyrosine nanocomposite (CAT). One gram of CuO nanoparticles was poured into 50 mL of distilled water and subjected to ultrasonication for 0.5 h. 100 mL of a 10 % solution of arginine was then infused into the resulting mixture of dispersion of CuO nanoparticles in distilled water and stirred vigorously for 6 h at 40 °C, followed by ultrasonication for 1 h. 100 mL of a 10 % solution of tyrosine (in H_2O) was then infused into the resulting mixture, followed by thorough stirring for 6 h at 40 °C and ultrasonication for 1 h. The product was washed twice, centrifuged and dried in the oven at 45 °C overnight to obtain CAT.

Characterization

The crystalline structure, crystallite size (*D*), full width at half maximum (FWHM) and morphological index (MI) of the synthesized CAT were determined from the X-ray diffraction studies using a powder X-ray diffractometer (Rigaku miniflex 600 by Rigaku Corporation, Japan). 45 kV was the operating voltage, while the current utilized was 40 mA. FTIR (Cary 630 by Agilent Technologies Inc) was carried out in the range of 4000 to 400 cm^{-1} to determine the functionalities present in CAT. The shape and morphology of CAT were studied using transmission electron microscopy (TEM). QUANTACHROME NOVA4200e, made in USA, Surface area analyser was used for BET analysis to describe the physical adsorption of nitrogen gas (*i.e.* adsorbate) molecules on CAT (adsorbent). The sample weight was 0.5 g and the outgas time was 3 h. Surface area and pore size distribution were determined from the analysis. The surface area of CAT was determined using multi-point BET (by N_2 adsorption), through parameters obtained from the BET plot [26]. Pore volume and pore size diameter were determined using the Barret-Joyner-Halenda (BJH) approach.

Electrochemical measurements

Electrochemical analyses were performed in 1 M HCl (electrolyte). An electrochemical assembly, consisting of mild steel (1 cm^2) functioning as the working electrode, a platinum rod as the counter electrode and a saturated calomel electrode (as reference electrode) was employed for electrochemical studies. The electrodes were connected to Autolab galvanostat/potentiostat electrochemical workstation, which in turn was connected to a computer. Mild steel of composition 98.835 wt.% Fe, 0.13 wt.% C, 0.18 wt.% Si, 0.39 wt.% Mn, 0.40 wt.% P; 0.04 wt.% S and 0.025 wt.% Cu was utilized in this study. To prevent charging current and confirm system stability, open circuit potential (OCP) was recorded for a duration of 30 minutes [27,28]. This is required for the metal to dissolve at its equilibrium or free potential, which is achieved at a stable OCP. Electrochemical impedance spectroscopic (EIS) measurements were performed between 100,000 and 0.01 Hz frequency range. Resistance to charge transfer (R_{ct}) values obtained from EIS were used to compute

the inhibition efficiency (IE) of CAT [29]. Potentiodynamic polarization (PP) measurements were determined in the interval of -250 and +250 mV, while the OCP scan rate (which is the pace at which the potential of mild steel changes as it is scanned) was set at 0.001 V s^{-1}.

Results and discussion

X-ray diffraction analysis

Peaks at 2θ= 7.9506, 13.5028, 15.2489, 17.9563, 19.9401, 20.3818, 21.6858, 24.7543, 25.7513, 27.0314 and 28.5392° in the XRD diffraction pattern for CAT (Figure 1) may likely be due to crystal planes in L-arginine and L-tyrosine [30,31]. The peaks at 2θ= 32.7304, 34.3223 and 38.1606° corresponds to the (110), (111) and (200) crystal planes in monoclinic CuO nanoparticles. Debye-Scherrer equation presented in Equation (1) was adopted to calculate the crystallite size [16].

$$D = \frac{k\lambda}{\beta \cos\theta} \quad (1)$$

In Equation (1), *D* denotes crystallite size, λ is the wavelength of X-ray (0.15406 nm), β is the XRD peak full width at half maximum (FWHM) in radians, *k* is the shape factor or Scherer's constant (0.9) and θ is Bragg's diffraction angle in radians [16]. The mean crystallite size was 39.5292 nm. In Equation (2) MI is the morphology index, $FWHM_h$ is the highest FWHM value determined from peaks and FWHMp is the FWHM for a specific or particular peak for which MI is determined. MI is directly proportional to *D,* as evident in Figure 2, suggesting uniformity and fineness of CAT.

$$MI = \frac{FWHMh}{FWHMh + FWHMp} \quad (2)$$

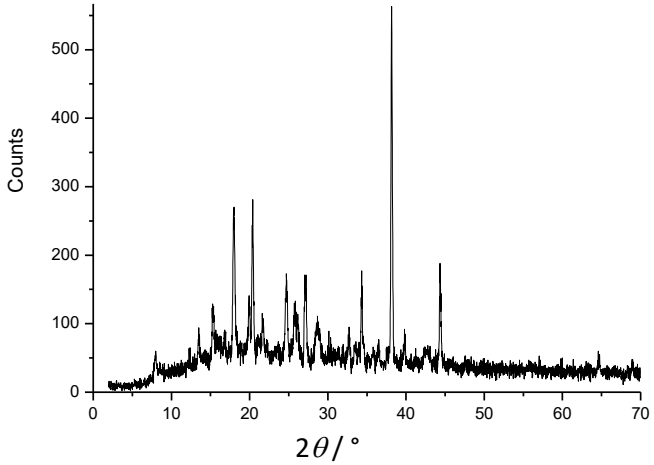

Figure 1. *XRD pattern of CAT*

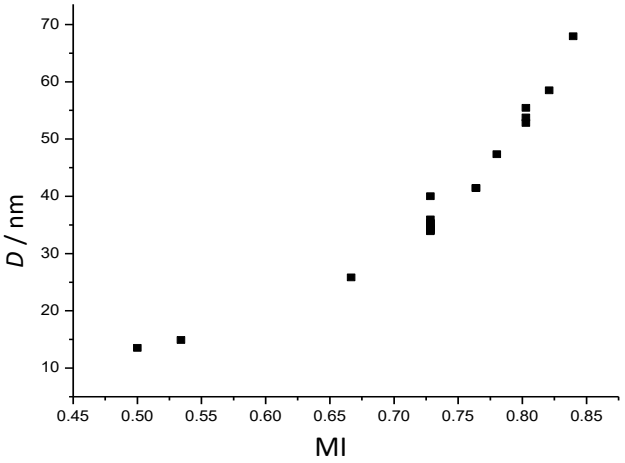

Figure 2. *Crystallite size vs. morphological index for CAT*

Transmission electron microscopic analysis

Transmission electron microscopy (TEM) creates images by detecting transmitted electrons. The TEM image of CAT presented in Figure 3 reveals semispherical-shaped nanoparticles with negligible agglomeration compared to highly agglomerated CuO nanoparticles, as reported by other researchers. The particle size ranges from 1.39 nm to 7.83 nm. The dispersed nature of CAT particles could be attributed to functionalization with amino acids. The observed spherical shape of the particles is consistent with other reports [32-34].

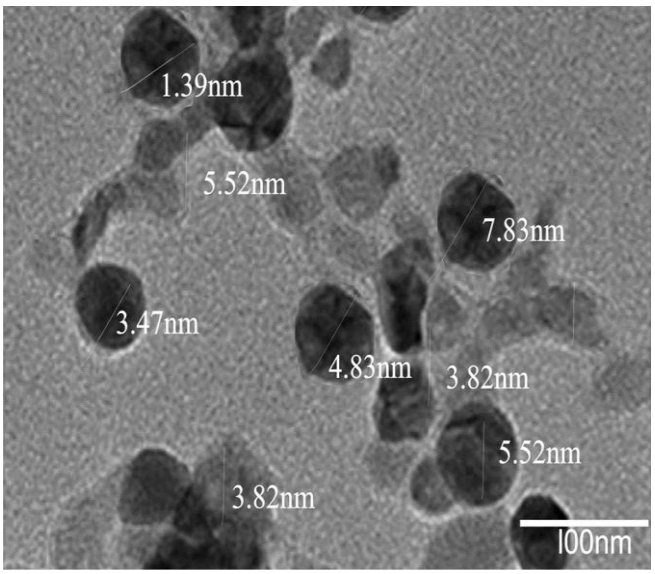

Figure 3. *TEM image for CAT*

Surface area, pore volume and pore diameter

Multi-point BET (by N_2 adsorption) was employed to determine the surface area of the CAT while pore volume and pore size diameter were determined using the Barret-Joyner-Halenda (BJH) approach. The quantity of gas adsorbed, $1/[W((P_o/P)-1)]$, *versus* relative pressure, P/P_o, is defined by Equation (3), and for CAT is presented in Figure 4. W is the weight of gas adsorbed, W_m is the weight of adsorbate as a monolayer, P is the pressure of the gas, P_o is the saturation vapour pressure at a given temperature and C is the BET constant. Figure 4 reveals that gas adsorption occurred at low relative pressure, suggesting that nitrogen gas molecules were principally adsorbed on small pores.

$$\frac{1}{W\left[\left(\frac{P_o}{P}\right)-1\right]}=\frac{1}{W_mC}+\frac{C-1}{W_mC}\frac{P}{P_o} \quad (3)$$

The multipoint BET surface area for CAT was 221 $m^2\ g^{-1}$. The pore volume and diameter were 0.0842 $cm^3\ g^{-1}$ and 2.137 nm, respectively. BJH studies revealed that CAT is mesoporous since the nanocomposite comprises pores having diameters within the range of 2 to 50 nm [35,36]. A material is classified as mesoporous when it contains pores between 2 and 50 nm in diameter.

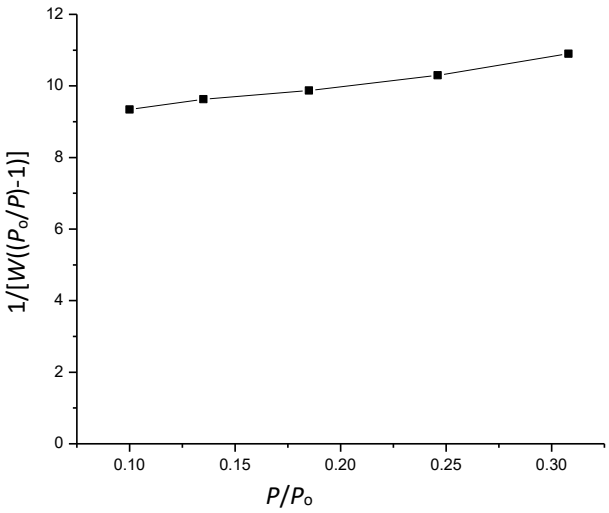

Figure 4. *Multi-point BET plot for CAT*

Fourier transform infrared spectroscopy analysis

The FTIR spectrum of CAT is presented in Figure 5. Generally, metal oxides show absorption bands between 600 and 400 cm^{-1} [37]. A peak was observed in this region, which could be due to Cu-O stretch. Peaks observed at 1561 cm^{-1} and 1360 cm^{-1} in the FTIR spectrum for CAT correspond to aromatic C=C stretching and C-N-H symmetric bending, respectively. The broad band around 3300 cm^{-1} could be due to O-H. The peak for phenolic C-O stretch was observed at 1244 cm^{-1}, while the C-O-H out-of-plane bending peak was observed at 875 cm^{-1} [38]. The peak at 738 cm^{-1} could be attributed to the out-of-plane bending of aromatic C-H. Some of the peaks arise from L-tyrosine and L-arginine [30,31,38]. The in-plane deformation of OH coupled to C-C bending vibration was observed at about 1360 cm^{-1} and is likely to arise from L-tyrosine [30].

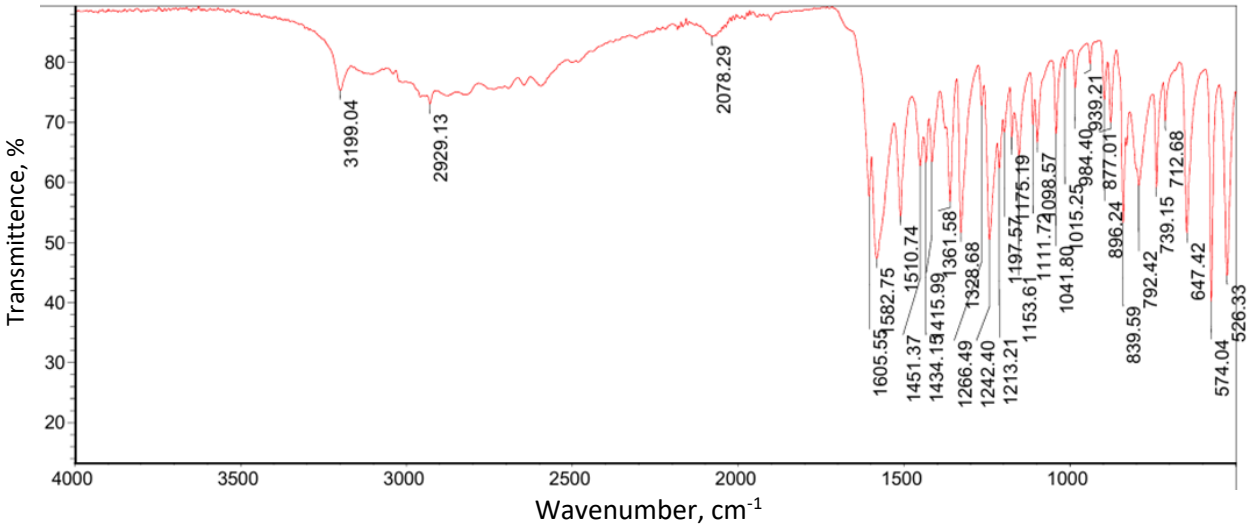

Figure 5. *FTIR spectrum of CAT*

Open circuit potential

Open circuit potential (OCP) analysis provides insight into the metallic corrosion inhibitory process. The potential under conditions of no current flow and no applied external voltage is called OCP. It is the potential developed between the mild steel surface (or any other metal surface) and the environment, with regard to a reference electrode positioned in electrolyte near the mild steel (which is a working electrode). Umoren *et al.* [39] defined OCP as the free corrosion potential (E_{corr}) when the system accomplishes an equilibrium, and zero-net electrical current flows through the mild steel surface. OCP reaches a steady-state value, E_{corr}, as the corrosion reaction approaches equilibrium. Plot of OCP versus time is imperative to comprehend the interaction of the mild steel surface in contact with its environment.

OCP *vs*. time plots for mild steel in blank 1 M HCl and with different concentrations of CAT are presented in Figure 6. The OCP–time profile reveals that the systems reached a stable OCP before the first 600 s after dipping in the corrosive medium. Thus, the 30-minute waiting period prior to electrochemical perturbations to stabilize the OCP is appropriate [28]. The conspicuous difference between the OCP values of the blank HCl and inhibited systems indicates that CAT has a reasonable impact on the electrochemical process taking place in the corrosive solution.

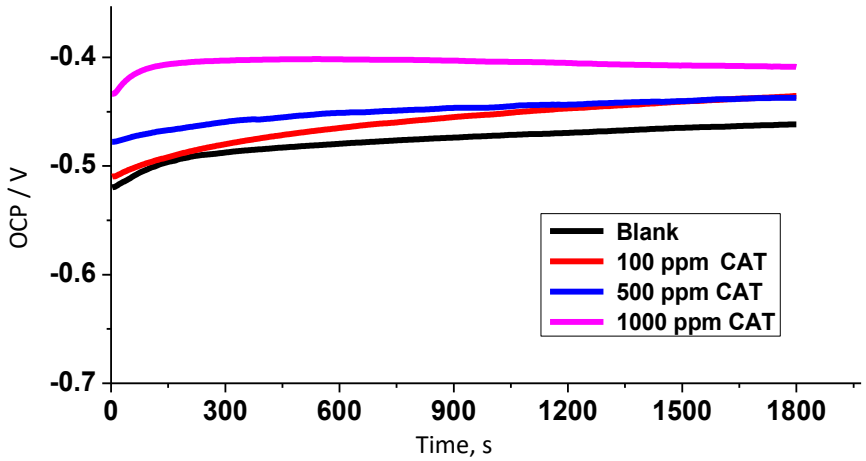

Figure 6. *OCP* vs. *time plots for MS in HCl in the presence and absence of CAT*

Electrochemical impedance spectroscopy

Electrochemical impedance spectroscopy (EIS) analysis can offer a reasonable description of the frequency response of a working electrode (mild steel in this case) in relation to electrochemical interactions at the electrode/electrolyte interface. The EIS spectra for mild steel in blank 1 M HCl and in the presence of CAT are presented in Figure 7, while the electrical equivalent circuit (EEC) employed to analyze EIS data is shown in Figure 8. The EEC includes solution resistance (R_s), resistance to charge transfer (R_{ct}), and constant phase element (CPE) involved to account for double-layer capacity effects. R_s denotes the resistance encountered by the electrolyte solution, whereas R_{ct} indicates the resistance to the specific electrochemical reaction occurring at the electrode interface. Radial frequency ($\omega = 2\pi f$) dependence of CPE impedance, $Z_{CPE}(\omega)=Y_o^{-1}(j\omega)^{-n}$, involves two frequency-independent parameters, Y_0 and n, where for n = 1, Y_0 becomes equal to pure double-layer capacitance.

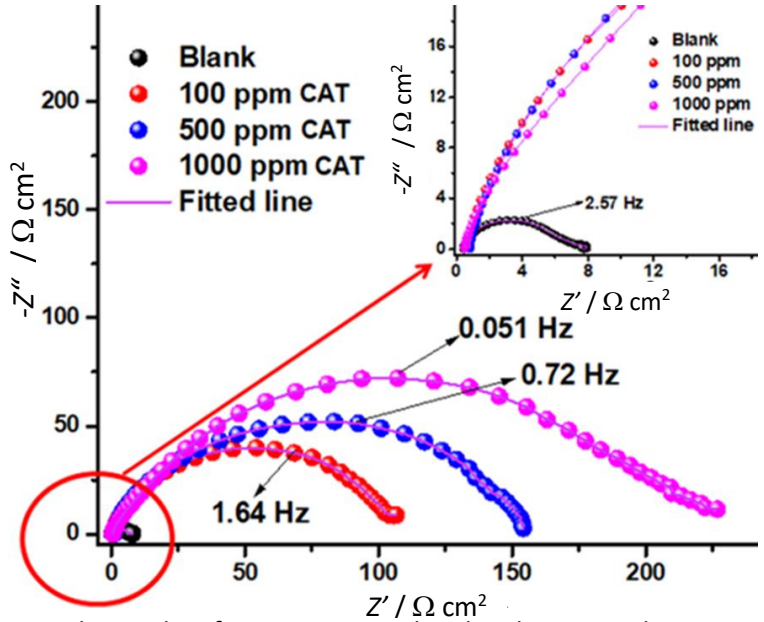

Figure 7. *Impedance plots for MS in 1 M HCl in the absence and presence of CAT*

The impedance diagrams are comprised of semicircles that are depressed and imperfect, which is typical of solid working electrodes, signifying frequency dispersions of interfacial impedance [40]. This very important attribute can be credited to adsorption of inhibitors, porous layer formation and coarse working electrode surface.

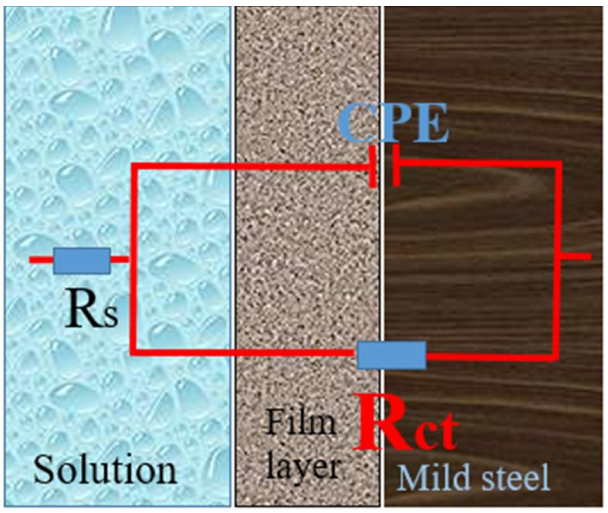

Figure 8. *Electrical equivalent circuit used to fit EIS data*

The marked similarities between the impedance spectra for mild steel recorded in blank 1 M HCl and in the presence of CAT are a clear indication that CAT did not alter the corrosion mechanism of mild steel in the aggressive medium [41]. The impedance plots revealed semicircles with increased diameters in the presence of CAT compared to those obtained for blank 1 M HCl. The consistent increase of semicircle diameters with an increase in concentration of CAT suggests an upsurge of R_{ct} values, and this could be due to an increased number of adsorbed inhibitor molecules (or surface coverage, Γ) on the mild steel surface [42].

Bode plots showing the effects of CAT concentration increase on mild steel corrosion in 1 M HCl are presented in Figure 9. The plots revealed increased area under the curves in the presence of CAT compared to that obtained in the absence of CAT [16]. This marked increase depends on the concentration of CAT. Also, an increase in the concentration of CAT increased the impedance modulus (at low frequencies) where R_{ct} dominates. Increase of R_{ct} values could be due to an increase in inhibitor molecules adsorbed on the mild steel surface, resulting in higher surface coverage [13].

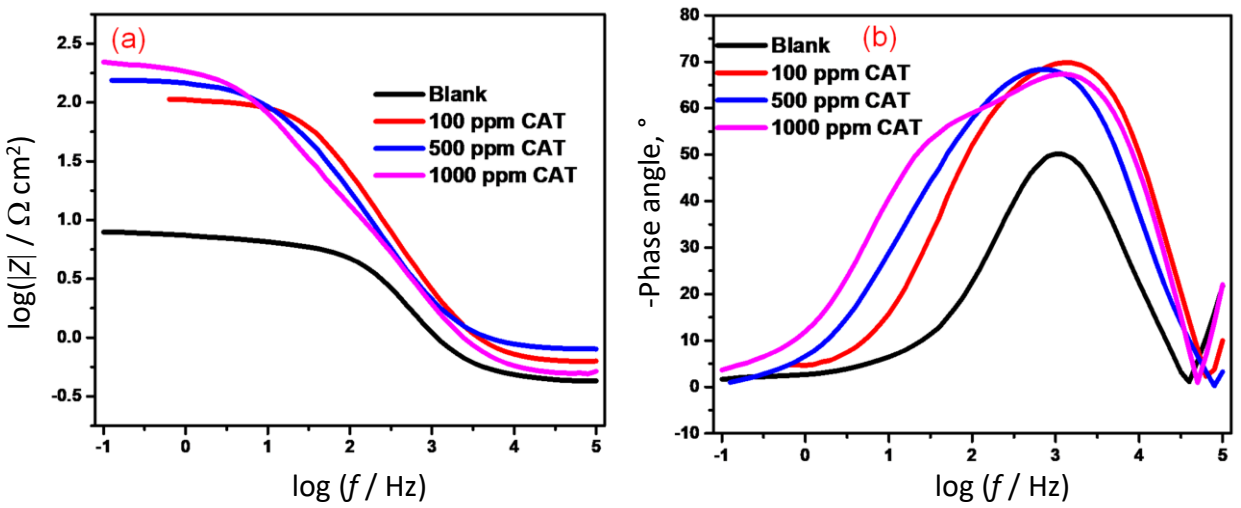

Figure 9. *(a) Bode magnitude and (b) phase angle plots for MS in 1 M HCl in the presence and absence of CAT*

The values of four impedance parameters (R_s, R_{ct}, Y_o and n) obtained by fitting EEC in Figure 8 to measured impedance spectra are summarized in Table 1. Charge transfer resistance (R_{ct}) values are greater in the presence of CAT compared to the uninhibited 1 M HCl, as shown in Table 1. The highest R_{ct} (226.80 Ω cm^2), accompanied by the lowest Y_0 value, was obtained in the presence of 1000 ppm CAT. This observation is consistent with other reports in the literature [16].

The R_{ct} values were employed to calculate inhibition efficiency using Equation (4). Generally, R_{ct} is a function of inhibition efficiency, since the increase in R_{ct} values in the presence of the inhibitor results in an increase in IE values.

$$IE = \frac{R_{ct} - R^{\circ}_{ct}}{R_{ct}} 100 \quad (4)$$

In Equation (4), R_{ct} is charge transfer resistance in the presence of CAT, while R°_{ct} is charge transfer resistance in the absence of the inhibitor.

Table 1. *Impedance parameter values and %IE for MS in 1M HCl in the absence and presence of CAT*

Inhibitor concentration, ppm	R_s / Ω cm^2	R_{ct} / Ω cm^2	n	Y_o / μΩ^{-1} s^n cm^{-2})	IE, %
0 (blank)	1.01	7.30	0.91	196.30	-
100	1.04	105.10	0.88	177.40	93.10
500	1.13	154.60	0.86	173.90	95.30
1000	1.08	226.80	0.84	168.70	96.80

Potentiodynamic polarization

Polarization plot for mild steel in the absence and presence of different concentrations of CAT is presented in Figure 10.

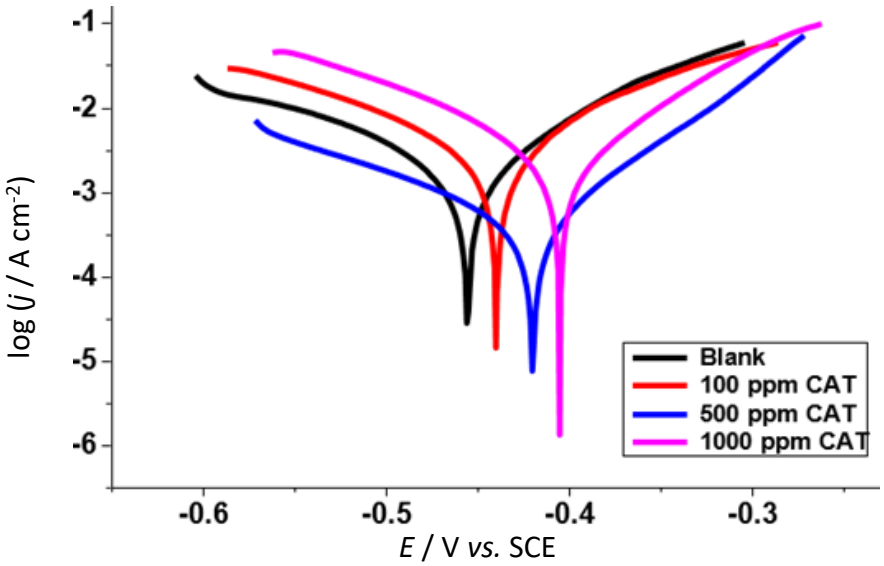

Figure 10. *Polarization plots for MS in 1 M HCl without and with CAT*

PP measurements disclosed that the presence of CAT diminishes current densities (j_{corr}) at the anodic and cathodic sites [18]. This remarkable decrease in j_{corr} in the presence of the studied inhibitor compared to the uninhibited system is a function of concentration and the greatest decrease in j_{corr} was recorded when 1000 ppm of CAT was introduced (Table 2). The consistent decrease in j_{corr} with the surge in CAT dosage could be due to an increase in a number of adsorbed CAT molecules on the mild steel surface. This finding corroborates results obtained from EIS measurements. It is important to note that j_{corr} values were used to calculate the inhibition efficiency with the aid of Equation (5).

$$IE = \frac{j^{0}_{corr} - j_{corr}}{j^{0}_{corr}} 100 \quad (5)$$

where j^{o}_{corr} is corrosion current density in the absence of inhibitor, while j_{corr} is corrosion current density in the presence of CAT.

The corrosion potential (E_{corr}), Tafel slopes (β_a, β_c), j_{corr}, and IE for CAT are presented in Table 2. According to the literature, if the change of E_{corr} is < 85 mV, the studied inhibitor is said to be a mixed-type inhibitor, and if the E_{corr} is > 85 mV, the inhibitor can be considered to behave as a cathodic or anodic type. Therefore, since the shift of E_{corr} is <85 mV, CAT demonstrated mixed type inhibitor propensity [43,44]. The corrosion potential is shifted to more positive values compared to the corrosion potential obtained for an uninhibited acid solution. In other words, the corrosion potential shifted towards the anode, suggesting that the introduction of CAT inhibits the anodic reaction more than the cathodic reaction. Thus, CAT acts as a mixed-type inhibitor with the predominant anodic influence. It is important to mention that the magnitude of decrease of current density in the presence of CAT is greater than that observed in the presence of copper oxide nanoparticles in a study conducted by Darweesh *et al*. [45]. Consequently, CAT exhibited higher inhibition efficiency compared to only copper oxide nanoparticles, which could be due to the presence of functionalities from amino acids.

Table 2: *Polarization parameters for MS in 1M HCl in the absence and presence of CAT*

Concentration, ppm	β_a / mV dec^{-1}	β_c / mV dec^{-1}	j_{corr} / µA cm^{-2}	E_{corr} / V	IE, %
0 (blank)	93.800	-78.100	492.600	-0.456	-
100	92.700	-79.200	68.100	-0.440	86.300
500	87.900	-80.400	52.200	-0.417	89.500
1000	90.300	-83.300	31.500	-0.405	93.700

Adsorption isotherm study

Experimental data generated from EIS and PP measurements were subjected to isotherm studies. This was done to establish the adsorption mode of CAT on the surface of mild steel in the aggressive acid medium [45]. The Langmuir adsorption isotherm model (Figure 11) gave a good line of fit for the adsorption process (Table 3), suggesting that the adsorption of CAT on the MS surface obeys the Langmuir isotherm [46]. The expression given by Equation (6) represents the isotherm model of Langmuir [46].

$$\frac{C}{\Gamma} = C + \frac{1}{K_{ads}} \tag{6}$$

where C signifies the concentration of the inhibitors, K_{ads} is the adsorption equilibrium constant and Γ denotes the surface coverage.

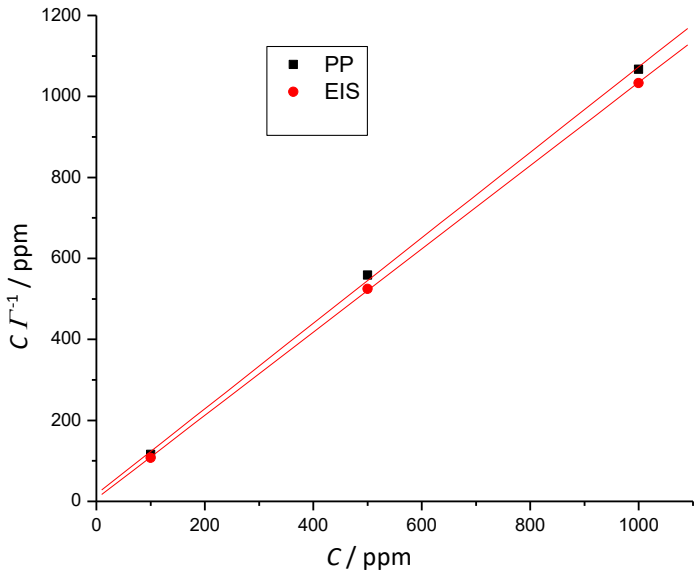

Figure 11. *Langmuir isotherm for CAT*

Table 3. *Linear regression parameters obtained for Langmuir isotherm plots in Fig. 11*

	Slope	Intercept	K_{ads} / ppm^{-1}	SD	R^2
EIS	1.02802	6.76574	0.15000	4.76671	0.99997
PP	1.05545	17.66508	0.05700	16.21405	0.99971

Orbital considerations and proposed inhibition mechanism

Frontier molecular orbital theory is an important model that allows for the prediction of chemical reactivity. The interactions between HOMO and LUMO are important in establishing how a molecule will interact with another molecule [47]. HOMO connotes the electron-donating area while LUMO represents the electron-accepting region within a molecule. Density functional theory (DFT) method at the hybrid functional Becke 3 Lee Yang Par (B3LYP) level of theory with 6-31G(D) basis set by Spartan 14 (version 1.2.0) program was employed to obtain HOMO and LUMO of tyrosine. The optimized structure, highest occupied molecular orbital (HOMO) and lowest unoccupied molecular orbital (LUMO) for tyrosine are presented in Figures 12a, 12b, and 12c respectively. The HOMO and LUMO of tyrosine are both delocalized on -C_6H_4-OH end and not on the whole molecule. The delocalization is more prominent in HOMO which suggest strong electrophilic tendency [13]. In CuO, the HOMO is located in the oxygen region (just like in ZnO), while the LUMO is located in the metal region [48].

Kaya *et al.* [49] reported their findings on quantum chemical and molecular dynamic simulation investigation on arginine and some amino acids. In arginine, the electron density in the HOMO is concentrated on the positively charged guanidine group, which is the key functional group responsible for the molecule's hydrogen bonding capabilities. The LUMO electron density is principally localized on the carbonyl group of carboxylic acid, rendering it the most predisposed site for accepting electrons in a chemical reaction. Theoretically, synergy between molecules with such interesting attributes would likely produce a good corrosion inhibitor. A good corrosion inhibitor should possess groups that would aid interaction between the metal and inhibitor molecules, resulting in the formation of a protective inhibitor film on the metal surface [20].

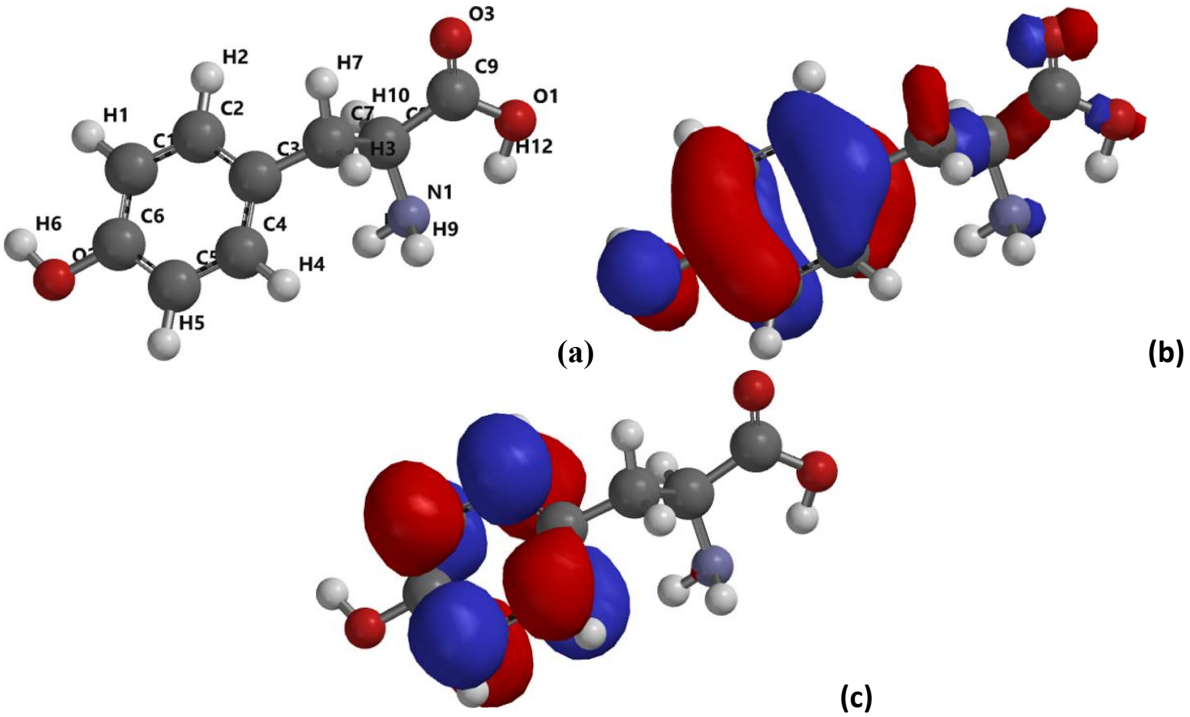

Figure 12*. (a) The optimized structure of tyrosine, (b) the highest occupied molecular orbital (HOMO), (c) the lowest unoccupied molecular orbital (LUMO)*

According to Chen *et al.* [50], in solutions of hydrochloric acid, introduced organic compounds have the potential to create a thin film on the surface of metals, thereby considerably diminishing the rate of corrosion. This phenomenon is understood as a substitution reaction occurring between the inhibitor molecules and the water molecules at the interface between the metal and the solution [50]. Given that L-tyrosine and L-arginine are both organic compounds classified as amino acids, it is possible that the nanocomposite, CAT, could create a thin layer on the metal surface, thereby markedly decreasing the corrosion rate. This reduction in corrosion rate may be facilitated by a substitution reaction between the inhibitor molecules and water molecules at the interface of the metal and the solution. Therefore, the retardation of mild steel deterioration in HCl by CAT may occur through a substitution reaction between molecules of CAT and molecules of H_2O at the metal/solution interface as presented in Equation (7) [16,50].

$$CAT_{(sol)} + aH_2O_{(ads)} \rightarrow CAT_{(ads)} + aH_2O_{(sol)} \quad (7)$$

$H_2O_{(ads)}$ is adsorbed H_2O molecules on the metal surface, $H_2O_{(sol)}$ signifies H_2O in solution, and *a* is the size ratio which indicates the number of H_2O molecules displaced by 1 molecule of CAT. $CAT_{(sol)}$ and $CAT_{(ads)}$ represent dissolved CAT in solution and molecules of adsorbed CAT on the surface of the metal, respectively [16].

In the presence of CAT, the mechanism of inhibition of anodic dissolution can be presented as shown in Equations (8) to (14).

$$Fe + H_2O \leftrightarrow FeH_2O_{(ads)} \quad (8)$$

$$FeH_2O_{(ads)} + CAT \leftrightarrow FeOH^-_{(ads)} + H^+ + CAT \quad (9)$$

$$FeH_2O_{(ads)} + CAT \rightarrow Fe\text{-}CAT_{(ads)} + H_2O \quad (10)$$

$$FeOH^-_{(ads)} \rightarrow FeOH^+_{(ads)} + e^- \quad (11)$$

$$Fe\text{-}CAT_{(ads)} \rightarrow Fe\text{-}CAT^+_{(ads)} + e^- \quad (12)$$

$$FeOH_{(ads)} + Fe\text{-}CAT^+_{(ads)} \leftrightarrow Fe\text{-}CAT_{(ads)} + FeOH^+ \quad (13)$$

$$(FeOH)^+ + H^+ \rightarrow Fe^{++} + H_2O \quad (14)$$

As evident in Equations (8) to (14), the corrosion of Fe in the aggressive acid solution rests on the adsorbed intermediate species. The lessening of the quantity of $FeOH^-_{(ads)}$ generated by Equation (9) owing to the replacement of H_2O by CAT in Equation 10 (leading to intermediate $FeCAT_{(ads)}$ formation) slows the rate-determining step (RDS), which is described by Equation (11). The retardation of the RDS retards corrosion of Fe [11,48].

Conclusions

The synthesized CuO nanoparticles/arginine/tyrosine nanocomposite tremendously suppressed the deterioration of mild steel in hydrochloric acid. The nanocomposite operated as a mixed-type inhibitor and caused a surge in charge transfer resistance. Inhibition efficiency increased with the increase in inhibitor dosage. The adsorption of the inhibitor on the mild steel surface obeyed the Langmuir isotherm model. CuO, arginine and tyrosine, characterized by their distinct chemical compositions, exhibit specific HOMO and LUMO properties that could play a significant role in corrosion inhibition. The presence of heteroatoms such as oxygen and nitrogen, coupled with the π-electrons associated with the aromatic ring in tyrosine, facilitates their interaction with metallic surfaces and thereby augments their capacity to inhibit corrosion. The mesoporous CuO nanoparticles/arginine/tyrosine exhibited reduced agglomeration, high surface area, and showed good potential as a mixed corrosion inhibitor for mild steel in hydrochloric acid.

Acknowledgements: *The inputs of Mr I. Yakubu of Chemical Engineering Department, Ahmadu Bello University Zaria, Dr V. I. Chukwuike of Federal University of Health Science, Uburu, Ebonyi State and Dr E. Ituen of Chemistry Department, University of Uyo, are acknowledged.*

References

[1] A. Anderez, F. J. Alguacil, F. A. López. Acid pickling of carbon steel, *Revista de Metalurgia* **58** (2022) e226. https://doi.org/10.3989/revmetalm.226

[2] M. C. Emesiani, V. C. Umegbolu, M. M. Mchihi. Corrosion inhibitory attributes of mixture of *codiaeum variegatum* and *ficus benjamina* for mild steel in hydrochloric acid medium, *Fudma Journal of Sciences* **8** (2024) 258-263. https://doi.org/10.33003/fjs-2024-0805-2677

[3] A. Toghan, O. K. Alduaij, N. Alqarni, E. M. Masoud, H. Alhussain, A. M. Mostafa, A. A. Farag, A. Fawzy. Mathematical, electrochemical, spectroscopic and microscopic monitoring of the adsorption effect of expired drugs on zinc corrosion in 3.5% NaCl solution, *Results in Chemistry* **13** (2025) 102006. https://doi.org/10.1016/j.rechem.2024.102006

[4] A. A. Farag, A. Toghan, Unravelling the adsorption and anti-corrosion potency of newly synthesized thiazole Schiff bases on C-steel in 1 M HCl: Computational and experimental implementations, *Results in Engineering* **25** (2025) 104504. https://doi.org/10.1016/j.rineng.2025.104504

[5] D-I. Răuță, E. Matei, S-M. Avramescu, Recent Development of Corrosion Inhibitors: Types, Mechanisms, Electrochemical Behavior, Efficiency, and Environmental Impact, *Technologies* **13** (2025) 103. https://doi.org/10.3390/technologies13030103

[6] D.T. Oyekunle, O. Agboola, A.O. Ayeni, Corrosion inhibitors as building evidence for mild steel: a review, *Journal of Physics: Conference Series* 1378 (2019) 032046. https://doi.org/10.1088/1742-6596/1378/3/032046

[7] S. Mahvidia, M. Gharagozloua, M. Mahdavianb, S. Naghibic, Potency of $ZnFe_2O_4$ Nanoparticles as Corrosion Inhibitor for Stainless Steel; the Pigment Extract Study. *Materials Research* **20** (2017) 1492-1502. http://dx.doi.org/10.1590/1980-5373-MR-2016-0772

[8] M. L. Zheludkevich, R. Serra, M. F. Montemor, G.S. Ferreira, Oxide nanoparticle reservoirs for storage and prolonged release of the corrosion inhibitors, *Electrochemistry Communications* **7** (2005) 836-840. https://doi.org/10.1016/j.elecom.2005.04.039

[9] E. Ituen, O. Akaranta, A. James, Elephant grass biomass extract as corrosion inhibitor for mild steel in acidic medium, *Journal of Material Science and Environmental Science* **8** (2017) 1498-1507. http://www.jmaterenvironsci.com

[10] N. W. Odozi, A. S. Adetoba, M. M. Mchihi, A. N. Akpaetok, *Synsepalum dulcificum* leaves extract as green inhibitor for mild steel corrosion in hydrochloric acid, *ChemSearch Journal* **12** (2021) 47-54. http://www.ajol.info/index.php/csj

[11] J. O. Madu, C. Ifeakachukwu, U. Okorodudu, F.V. Adams, I.V. Joseph, Corrosion Inhibition Efficiency of *Terminalia Catappa* Leaves Extracts on Stainless Steel in Hydrochloric Acid, *Journal of Physics: Conference Series* **1378** (2019) 022092. https://doi.org/10.1088/1742-6596/1378/2/022092

[12] A. Ezzat, S. M. Motaal, A. S. Ahmed, H. B. Sallam, A. El-Hossiany, A. S. Fouda. Corrosion Inhibition of Carbon Steel in 2.0M HCl Solution Using Novel Extract (*Pulicaria undulate*). *Biointerface Research in Applied Chemistry* **12** (2022) 6415-6427. https://doi.org/10.33263/BRIAC125.64156427

[13] M.M. Mchihi, N.W. Odozi, A.O. Nurudeen, M.C. Emesiani, B. O. Seriki. Assessment of Helianthus tuberosus leaves extract as eco-friendly corrosion inhibitor for Aluminum in sodium hydroxide: Insights from electrochemical, gravimetry and computational consideration, *Moroccan Journal of Chemistry* **12** (2024) 1462-1483. https://doi.org/10.48317/IMIST.PRSM/morjchem-v12i4.49160

[14] R. Aslam, M. Mobin, M. Shoeb, J. Aslam. Novel ZrO_2-glycine nanocomposite as eco-friendly high temperature corrosion inhibitor for mild steel in hydrochloric acid solution, *Scientific Reports* **12** (2022) 9274. https://doi.org/10.1038/s41598-022-13359-y
[15] P. Burhagohain, G. Sharma. A Descriptive study on the use of nanomaterials as corrosion inhibitors in oil and gas industry, *International Journal of Scientific & Technology Research* **8** (2019) 3999-4002.
[16] M. M. Mchihi, A. M. Olatunde, N. W. Odozi. Ficus sur mediated synthesis of mesoporous ZnO nanoparticles and novel ZnO/Arginine/Tyrosine nanocomposite as eco-friendly corrosion inhibitors for mild steel in hydrochloric acid medium, *Moroccan Journal of Chemistry* **12** (2024)1122-1152. https://doi.org/10.48317/IMIST.PRSM/morjchem-v12i3.42782
[17] L. Hamadi, S. Mansouri, K. Oulmi, A. Kareche, The use of amino acids as corrosion inhibitors for metals: A review, *Egyptian Journal of Petroleum* **27** (2018) 1157-1165. https://doi.org/10.1016/j.ejpe.2018.04.004
[18] B. E. Ibrahimi, A. Jmiai, L. Bazzi, S. E. Issami, Amino acids and their derivatives as corrosion inhibitors for metals and alloys, *Arabian Journal of Chemistry* **13** (2020) 740-771. http://dx.doi.org/10.1016/j.arabjc.2017.07.013.
[19] M. M. Khowdiary, N. A. Taha, N. M. Saleh, A. A. Elhenawy, Synthesis of Novel Nano-Sulfonamide Metal-Based Corrosion Inhibitor Surfactants, *Materials* **15** (2022) 1146. https://doi.org/10.3390/ma15031146
[20] F. Chioma, N. W. Odozi, M. M. Mchihi, M. A. Olatunde, Synthesis, spectroscopic, and density functional theory studies of the corrosion inhibitive behaviour of *n*-(1,4-dihydro-1,4-dioxonaphthalene-3-yl)pyrazine-2-carboxamide chelator-ligand, *Global Journal of Pure and Applied Sciences* **28** (2022) 39-50. https://dx.doi.org/10.4314/gjpas.v28i1.6
[21] S. H. Alrefaee, K. Y. Rhee, C. Verma, M. A. Quraishi, E. E. Ebenso, Challenges and advantages of using plant extract as inhibitors in modern corrosion inhibition systems: Recent advancements, *Journal of Molecular Liquids* **321** (2021) 114666. https://doi.org/10.1016/j.molliq.2020.114666
[22] N. Baig, I. Kammakakam, W. Falath, Nanomaterials: a review of synthesis methods, properties, recent progress, and challenges, *Materials Advances* **2** (2022) 1821-1871. https://doi.org/10.1039/d0ma00807a
[23] N. W. Odozi, M. M. Mchihi, M. A. Olatunde. Review of Recent Advances in Plant-Mediated Synthesis and Applications of $3d^6$ - $3d^{10}$ Metal Oxide Nanoparticles and their Composites, *Dutse Journal of Pure and Applied Sciences* **9(4b)** (2023) 91-120. https://www.ajol.info/index.php/dujopas/article/view/262332
[24] D. R. Mohammedali, H. I. Salman, M. N. Bahjat, E. S. Abood, Synthesis of new Corrosion Inhibitor from Nano-Polymer and study its adsorption on carbon steel at different Temperatures, *Egyptian Journal of Chemistry* **65** (2022) 691-705. https://dx.doi.org/10.21608/EJCHEM.2022.139171.6113
[25] A. Kasprzhitskii, G. Lazorenko, T. Nazdracheva, V. Yavna, Comparative computational study of l-amino acids as green corrosion inhibitors for mild steel, *Computation* **9** (2021) 1. https://dx.doi.org/10.3390/computation9010001
[26] A. A. Barzinjy, H. H. Azeez, Green synthesis and characterisation of zinc oxide nanoparticles using Eucalyptus globulus Labill. leaf extract and zinc nitrate hexahydrate salt, *Springer Nature Journal* **2** (2020) 991. https://doi.org/10.1007/s42452-020-2813-1
[27] J.M. Falcón, F.F. Batista, I.V. Aoki, Encapsulation of dodecylamine corrosion inhibitor on silica nanoparticles, *Electrochimica Acta* **124** (2014) 109-118. https://doi.org/10.1016/j.electacta.2013.06.114
[28] M. M. Mchihi, N. W. Odozi, S. A. Gbolahan, Electrochemical investigation of the inhibitory effect of zinc oxide nanoparticles/tenofovir disoproxil fumarate nanocomposite on mild steel

corrosion in 1 M hydrochloric acid, *Analytical and Bioanalytical Electrochemistry* **16** (2024) 559-567. https://doi.org/10.22034/ABEC.2024.714079

[29] H. Hamani, D. Daoud, S. Benabid, T. Douadi, M. Al-Noaimi, Investigation on corrosion inhibition and adsorption mechanism of azomethine derivatives at mild steel/0.5M H2SO4 interface: Gravimetric, electrochemical, SEM and EDX studies. *Journal of the Indian Chemical Society* **99** (2022) 100330. https://doi.org/10.1016/j.jics.2021.100330

[30] Y. Wang, Y. Chang, L. Yin, Y. Xue, Z. Li, C. Xue, A Novel Technological Process of Extracting L-Tyrosine with Low Fluorine Content from Defatted Antarctic Krill (*Euphausia superba*) By-product by Enzymatic Hydrolysis. *Food and Bioprocess Technology* **9** (2015) 621-627. https://doi.org/10.1007/s11947-015-1658-x

[31] S. N. Dalhatu, K. A. Modu, A. A. Mahmoud, Z. U. Zango, A. B. Umar, F. Usman, J. O. Dennis, A. Alsadig, K. H. Ibnaouf, O. A. Aldaghri, L-Arginine Grafted Chitosan as Corrosion Inhibitor for Mild Steel Protection, *Polymers* **15** (2023) 398. https://doi.org/10.3390/polym15020398

[32] W. W. Andualem, F. K. Sabir, E. T. Mohammed, H. B. Hadgu, A. G. Bedasa, Synthesis of copper oxide nanoparticles using plant leaf extract of *Catha edulis* and its antibacterial activity, *Journal of Nanotechnology* **2020** (2020) 2932434. https://doi.org/10.1155/2020/2932434

[33] S. N. Begum, A. Esakkiraja, S. M. Asan, M. Muthumari, G. V. Raj, Green Synthesis of Copper Oxide Nanoparticles Using Catharanthus Roseus Leaf Extract and Their Antibacterial Activity, *International Journal of Scientific Research in Multidisciplinary Studies* **5** (2019) 21-27.

[34] K. S. Devi, A. R. Singh, D. Velmurugan, D. Devi, D. S. Lourembam, N. R. Singh, Green Synthesis of Copper Oxide Nanoparticles Using Coix lacryma jobi Leaves Extract and Screening of its Potential Anticancer Activities, *Journal of Pharmaceutical Research International* **33** (2021) 128-139. https://doi.org/10.9734/JPRI/2021/v33i52A33566

[35] M. A. Ismail, K. K. Taha, A. Modwi, L. Khezami, ZnO Nanoparticles: Surface and X-Ray Profile Analysis, *Journal of Ovonic Research* **14** (2018) 381-393.

[36] N. A. Jadhav, P. K. Singh, H. W. Rhee, B. Bhattacharya, Effect of variation of average pore size and specific surface area of ZnO electrode (WE) on efficiency of dye-sensitized solar cells, *Nanoscale Research Letter* **9** (2014) 575. http://www.nanoscalereslett.com/content/9/1/575

[37] S. Fakhari, M. Jamzad, K. H. Fard, Green synthesis of zinc oxide nanoparticles: a comparison. *Green Chemistry Letters and Reviews* **12** (2019) 19-24. https://doi.org/10.1080/17518253.2018.1547925

[38] S. Kumar, S. B. Rai, Spectroscopic studies of L-Arginine molecule, *Indian Journal of Pure and Applied Physics* **48** (2009) 251-255.

[39] P. S. Umoren, D. Kavaz, S. A. Umoren, Corrosion Inhibition Evaluation of Chitosan-CuO Nanocomposite for Carbon Steel in 5% HCl Solution and Effect of KI Addition, *Sustainability* **14** (2022) 7981. https://doi.org/10.3390/su14137981

[40] E. Ituen, E. Ekemini, L. Yuanhuaa, R. Lia, A. Singh, Mitigation of microbial biodeterioration and acid corrosion of pipework steel using *Citrus reticulata* peels extract mediated copper nanoparticles composite, *International Biodeterioration & Biodegradation* **149** (2020) 1049352. https://doi.org/10.1016/j.ibiod.2020.104935

[41] M. Allaoui, O. Rahim, L. Sekhri, Electrochemical Study on Corrosion Inhibition of Iron in acidic medium by Moringa oleifera extract, *Oriental Journal of Chemistry* **33** (2017) 637-646. http://dx.doi.org/10.13005/ojc/330211

[42] R. A. Hameed, M. Faride, M. Othman, B. Huwaimel, S. Al-Mhyawi, A. Shamroukh, F. Alshammary, E. Aljuhani, M. Abdallah, Green synthesis of zinc sulfide nanoparticles-organic heterocyclic polyol system as eco-friendly anti corrosion and anti-bacterial corrosion inhibitor for steel in acidic environment, *Green Chemistry Letters and Reviews* **15** (2022) 847-862. https://doi.org/10.1080/17518253.2022.2141585

[43] N. W. Odozi, R. Saheed, M. M. Mchihi, Application of *peperomia pellucida* leaves extract as a green corrosion inhibitor for mild steel in 1.0 M hydrochloric acid solution, *ChemSearch Journal* **10** (2019) 88-93. http://www.ajol.info/index.php/csj

[44] N. W. Odozi, M. C. Emesiani, C. D. Charles, B. O. Seriki, M. M. Mchihi, Electrochemical studies of the corrosion inhibitory potential of *Annona muricata* leaves extract on aluminum in hydrochloric acid medium, *FUDMA Journal of Sciences* **8** (2024) 395-401. https://doi.org/10.33003/fjs-2024-0803-2460

[45] M. A. Darweesh, S. M. Emam, A. M. Wahba, M. I. Ayad, M. N. El-Nahass, A. S. Abd-Elhamied, W. A. Hammad, Onion peel extract/copper oxide nanoparticles as corrosion inhibitors for carbon steel in hydrochloric acid: Extraction, characterization, electrochemical study, and theoretical explorations, *Results in Chemistry* **9** (2024) 101626. https://doi.org/10.1016/j.rechem.2024.101626

[46] M. M. Mchihi, M. C. Emesiani, J. I. Babawumi, Inhibitory Potentials of Leaf Extract of Justicia Schimperi for Mild Steel Corrosion in Hydrochloric Acid Medium: Gravimetric, Microscopic and Spectroscopic Studies, *Asian Research Journal of Current Science* **5** (2023) 184-192. https://www.jofscience.com/index.php/ARJOCS/article/view/19

[47] K. Tarfaoui, N. Brhadda, M. Ouakki, M. Galai, E. Ech-chihbi, K. Atfaoui, M. Khattabi, M. Nehiri, R. Lachhab, M. Ebn Touhami, M. Ouhssine, Natural Elettaria cardamomum Essential Oil as a Sustainable and a Green Corrosion Inhibitor for Mild Steel in 1.0 M HCl Solution: Electrochemical and Computational Methods, *Journal of Bio- and Tribo-Corrosion* **7** (2021) 131. https://doi.org/10.1007/s40735-021-00567-8

[48] N. I. Oktavianti, G. R. Anindika, A. L. Ivansyah, Y. Kusumawati. Theoretical study of nickel-doped zinc oxide interaction with methylene blue and methyl orange using DFT methods. *Materials Research Express* **9** (2022) 125505. https://doi.org/10.1088/2053-1591/aca747

[49] S. Kaya, B. Tüzün, C. Kaya, I. B. Obot, Determination of Corrosion inhibition effects of amino acids: Quantum chemical and molecular dynamic simulation study, *Journal of the Taiwan Institute of Chemical Engineers* **58** (2016) 528-535. https://doi.org/10.1016/j.jtice.2015.06.009

[50] L. Chen, D. Lu, Y. Zhang, Organic Compounds as Corrosion Inhibitors for Carbon Steel in HCl Solution: A Comprehensive Review, *Materials* **15** (2022) 2023. https://doi.org/10.3390/ma15062023